Published in final edited form as:
Biochemistry. 2010 December 7; 49(48): 10287–10297. doi:10.1021/bi100500m.

Intrinsically disordered PEP-19 confers unique dynamic properties to apo and calcium calmodulin

Xu Wang, **Quinn K. Kleerekoper**, **Liang-wen Xiong**, and **John A. Putkey***
Department of Biochemistry and Molecular Biology and the Structural Biology Center, University of Texas, Houston Medical School, Houston, Texas 77030

Abstract

PEP-19 (Purkinje cell protein 4) is an intrinsically disordered protein with an IQ calmodulin (CaM) binding motif. Expression of PEP-19 was recently shown to protect cells from apoptosis and cell death due to Ca^{2+} overload. Our initial studies showed that PEP-19 causes novel and dramatic increases in the rates of Ca^{2+} association and dissociation from the C-domain of CaM. The goal of this work was to study interactions between C-domain of CaM (C-CaM) and PEP-19 by solution NMR to identify mechanisms by which PEP-19 regulates Ca^{2+} binding to CaM. Our results show that PEP-19 causes a greater structural change in apo C-CaM relative to Ca^{2+}-C-CaM, and that the 1st Ca^{2+} binds preferentially to site IV in the presence of PEP-19 with exchange characteristics that are consistent with a decrease in Ca^{2+} binding cooperativity. Relatively weak binding of PEP-19 has distinct effects on chemical/conformational exchange on the μs-ms timescale. In apo C-CaM, PEP-19 binding causes a redistribution of residues that experience conformational exchange, leading to an increase in residues around Ca^{2+} binding site IV that undergo conformational exchange on μs-ms timescale. This appears to be due to an allosteric effect since these residues are not localized to the PEP-19 binding site. In contrast, PEP-19 increases the number of residues that exhibit conformational exchange in Ca^{2+}-C-CaM. These residues are primarily localized to the PEP-19 binding site, but also include Asp93 in site III. These results provide working models for the role of protein dynamics in regulation of Ca^{2+} binding to CaM by PEP-19.

PEP-19 (Purkinje cell protein 4) is a small 6.7 kDa polypeptide that was initially identified in the central nervous system (CNS), but is now known to be present in a variety of other tissues (for review see (1–5)). PEP-19 has no known intrinsic activity other than binding to calmodulin (CaM) in the presence or absence of Ca^{2+} via an IQ CaM binding motif. This gives PEP-19 the potential to exert broad cellular effects as a regulator of CaM signaling. This idea is consistent with a general cytoprotective role for PEP-19 put forth based on the fact that Purkinje cells of the cerebellum and granule-cell neurons in the dentate gyrus, which have high levels of PEP-19, are largely spared from the effects of Alzheimer's Disease, while PEP-19 negative cells are severely affected (6). Conversely, cell types that are most affected by Huntington's disease exhibit a significant loss of expression of PEP-19 (7). Experimental studies also support a cytoprotective role for PEP-19 since expression of PEP-19 greatly inhibits cell death due to apoptosis (8,9), or glutamate-induced Ca^{2+} cytotoxicity (9). Interestingly, PEP-19 is greatly increased in human leiomyoma versus matched myometrium (10), and high levels of PEP-19 are found in 58 of 60 NCI-60 tumor cell lines (11), even cells derived from tissues that express low or no PEP-19. This may be related to increased survival potential of transformed cells due to antiapoptotic effects of

*Corresponding author. 6431 Fannin St., Houston, TX 77030. john.putkey@uth.tmc.edu; Phone: 713-500-6061; Fax: 713-500-0652;.

PEP-19. These observations support the idea that PEP-19 protects cells against apoptosis and Ca^{2+} cytotoxicity due to normal or pathogenic conditions, and would explain the need for high levels of PEP-19 in cells with highly active Ca^{2+} signaling systems.

The potential for PEP-19 to function as a regulator of CaM signaling led us to a series of studies to characterize its structural and biochemical properties, and its effects on CaM. We showed that PEP-19 binds relatively weakly, but selectively to the C-domain of CaM and has novel effects on the Ca^{2+} binding properties of CaM (12). Specifically, PEP-19 causes a 40-fold increase in the rates of association (k_{on}) and dissociation (k_{off}) of Ca^{2+} at C-domain of CaM, with little effect on Ca^{2+} binding affinity. Selective effects on the C-domain of CaM are important since the k_{on} and k_{off} for Ca^{2+} binding to the C-domain are up to 150-fold slower than for the N-domain, and represent a rate-limiting step for activation of Ca^{2+}-dependent target proteins. We also showed that PEP-19 is intrinsically disordered, but with residual structure localized to an acidic/IQ motif that includes the IQ sequence and an adjacent acidic sequence (13). The core IQ motif is required for binding to CaM, but the acidic region is necessary to restrict binding to the C-domain, and for modulating Ca^{2+} binding to CaM (14).

The C-domain of CaM has intriguing dynamic properties that may act in synergy with the intrinsic disorder of PEP-19. Protein dynamics from NMR showed that the C-domain of CaM presents an ensemble of conformational states. The “open” conformation is dominant in the presence of Ca^{2+}, and the “closed” conformation dominates in the apo state, but other minor populations of intermediate states exist (15–17). Akke and colleagues showed that the rate of Ca^{2+} exchange in the C-domain CaM is correlated with rates of chemical/conformational exchange (18). Thus, binding targets to CaM provides a mechanism for altering its Ca^{2+} binding properties by changing its dynamic properties and the populations of CaM conformers. For example, binding high-affinity targets to Ca^{2+}-CaM, shifts the conformational equilibrium by stabilizing an “open-like” Ca^{2+}-bound conformation, which greatly decreases k_{off} (19). Based on these observations, we propose an inverse mechanism in which low affinity binding of intrinsically disordered PEP-19 modulates the slow dynamics of apo CaM and Ca^{2+}-bound CaM to increase Ca^{2+} binding rate constants.

The present study provides experimental evidence to validate the above hypothesis by investigating the effects of PEP-19 on backbone dynamics of the isolated C-domain of CaM (C-CaM). In contrast to high-affinity CaM binding peptides, PEP-19 binding increases slow motions in the C-domain of CaM. In particular, residues located in Ca^{2+} binding sites in both apo- and Ca^{2+}-bound forms undergo conformational exchange on us-ms timescale. This provides working models for the structural and dynamic basis for the effect of PEP-19 on the kinetics of Ca^{2+} binding to CaM.

MATERIALS AND METHODS

Protein purification

Recombinant CaM and PEP-19 were cloned, expressed in bacteria and purified as described previously (12,13,20,21). A bacterial expression vector for C-CaM (residues 76–148) was kindly provided by Dr. Madeline Shea (U. Iowa). Proteins were decalcified by addition of 5 mM EGTA and 0.1 mM BAPTA followed by desalting on a Biorad P6DG or P2DG size exclusion column into a buffer that was decalcified by passage over a calcium-sponge column (Molecular Probes). Protein concentrations were estimated using an extinction coefficient of $\varepsilon_{276nm} = 0.18\ ml^{-1}/mg$ for CaM, and $\varepsilon_{215nm} = 0.59\ ml^{-1}/mg$ for PEP-19, or by using the BCA protein assay (Pierce). More precise concentrations of CaM and C-CaM were determined by measuring the amount of Ca^{2+} released from the C-domain of Ca^{2+}-saturated proteins. Briefly, a solution of approximately 2 μM CaM or C-CaM and 30 μM Ca^{2+} was

rapidly mixed with a solution of 300 μM of the Ca^{2+} sensitive dye, Quin-2, using a stopped flow fluorimeter to monitor the slow release of Ca^{2+} from the C-domain as described previously (12). The amount of Ca^{2+} released from the sample was determined by calibrating the fluorescence response with EGTA standards. This was then used to calculate the concentration of CaM or C-CaM.

Equilibrium Ca^{2+} titrations monitored by tyrosine fluorescence

Equilibrium Ca^{2+} binding constants for CaM and C-CaM in the presecnce or absence of PEP-19 were determined using tryosine fluoresence as described previously (22). Solutions containing 20 mM MOPS, pH 7.5, 100 mM KCl, 1 mM EGTA, 1 mM HEDTA, 1 mM NTA, 5 μM CaM or C-CaM with or without 30 μM PEP-19 were titrated with a Ca^{2+} stock to achieve a wide range of free Ca^{2+}. The concentration of total Ca^{2+} needed to achieve a desired free Ca^{2+} concentration was determined using the online calculator MaxChelator (http://www.stanford.edu/~cpatton/maxc.html). The Ca^{2+} stock was prepared in the same buffer, including proteins, such that only the concentration of Ca^{2+} was changed during the titration. Tyrosine fluorescence intensity was plotted against the free Ca^{2+} concentration and fit to the following form of the Hill equation:

$$F = F_{\min} + (F_{\max} - F_{\min}) \left[\frac{[\mathrm{Ca}]^n}{[\mathrm{Ca}]^n + [k_{\mathrm{Ca}}]^n} \right] \quad (1)$$

where $[Ca^{2+}]$ is the free Ca^{2+} concentration, F is the fluorescence intensity at a given free Ca^{2+} concentration, F_{min} is the initial fluorescence intensity in the absence of added Ca^{2+}, F_{max} is the fluorescence at maximal Ca^{2+}, k_{Ca} is the concentration of Ca^{2+} at which the change in fluorescence is half maximal and n is the Hill coefficient.

NMR methodology

All NMR experiments were performed on a Bruker DRX 600 MHz spectrometer equipped with a 5 mm triple-resonance cryoprobe at 298 K. NMR samples were prepared using decalcified proteins in a buffer containing 10 mM imidazole, 100 mM KCl and 5% D_2O at pH 6.3. Samples used for relaxation measurements and backbone assignments contained 0.5 mM C-CaM uniformly labeled with ^{15}N or $^{13}C/^{15}N$, with or without 0.7 mM PEP-19. Excess EDTA or $CaCl_2$ was added to maintain apo or Ca^{2+}-bound states, respectively.

Backbone assignments for C-CaM/PEP-19 for apo and Ca^{2+}-bound states were obtained using the following 3D experiments: HNCO, HNCA, HN(CO)CA, HNCACB, CBCA(CO)NH, ^{15}N HSQC-TOCSY and ^{15}N-edited NOESY-HSQC experiments. The ^{15}N longitudinal (R_1), transverse (R_2) relaxation rate constants and heteronuclear $[^1H]$-^{15}N NOE were acquired using published pulse sequences (23). Experiments were recorded at delays of 20, 100, 200, 400, 600, 800, 1000, 1200, and 1400 ms for R_1 measurements, and delays of 16.96, 33.92, 50.88, 67.84, 84.8, 118.72, 135.68, 152.64, and 169.6 ms for R_2 measurements. $[^1H]$-^{15}N NOE values were measured from spectra with and without proton saturation recorded in an interleaved manner. Proton saturation was acquired using a 120° ^1H pulse applied every 5.0 s. In the case of the NONOE spectra, a net relaxation delay of 5.0 s was employed, while a relaxation delay of 2.0 s prior to a 3.0 s proton presaturation period was employed for the NOE spectra.

All NMR spectra were processed and analyzed using Topspin 2.0 (Bruker) and FELIX 2004 (MSI, San Diego, CA). ^1H chemical shifts were referenced to DSS (2,2-dimethyl-2-silapentane-5-sulphonate), and $^{15}N/^{13}C$ chemical shifts were referenced indirectly using

their respective gyromagnetic ratios (24). The average amide chemical shift change ($\Delta\delta_{avg}$) was calculated using the following equation:

$$\Delta\delta_{avg}=\sqrt{\frac{(\Delta\delta\mathrm{H})^2+(\Delta\delta\mathrm{N}/5)^2}{2}} \quad (2)$$

Where Δδ H and Δδ N are the changes in ^{1}H and ^{15}N chemical shifts, respectively.

Analysis of relaxation data

Values for R_1, R_2 and their uncertainties were derived by plotting peak intensity versus delay time and fitting the data to a single exponential decay equation using non-linear least squares analysis. [^{1}H]-^{15}N NOE values were calculated from the ratios of peak intensities with and without presaturation. The standard deviation of the NOE was calculated from the root mean square value of the background noise in the spectra (23).

Reduced spectral density mapping was used to analyze the relaxation data (25,26). Values for $J(0)$, $J(\omega_N)$, and

$$J(\omega_H) \approx J(\omega_H+\omega_N) \approx J(\omega_H-\omega_N) \quad (3)$$

$$R_{NOE}=(NOE-1)R_1(\gamma_N/\gamma_H) \quad (4)$$

$$J(0)=(-0.75R_1+1.5R_2-0.9R_{NOE})/E \quad (5)$$

$$J(\omega_N)=(R_1-1.4R_{NOE})/E \quad (6)$$

$$J(\omega_H)=R_{NOE}/5A \quad (7)$$

$$E=3A+C^2 \quad A=(\mu_0 h\gamma_H\gamma_N/16\pi^2 r_{NH}^3)^2 \quad C=(\omega_N/\sqrt{3})(\sigma_\parallel-\sigma_\perp)$$

Where μ_0 is the permeability of free space, h is Plank's constant, γ_H and γ_N are the gyromagnetic ratios of ^{1}H and ^{15}N, respectively, r_{NH} is the average N-H bond length (1.02 Å). Uncertainties in the spectral density parameters were estimated using 500 Monte Carlo simulations based on the uncertainties in the measured relaxation parameters.

Residue-specific rotational correlation times ($\boldsymbol{\tau}_m$) were estimated from the ratio of R_2/R_1 (27) (software r2r1_tm, A. G. Palmer III, Columbia University). Residues with R_2/R_1 ratios falling outside one standard deviation (SD) of the mean, as well as residues with NOE < 0.65, were excluded from the analysis (28).

RESULTS

C-CaM is a valid structural model for studying interactions between CaM and PEP-19

We showed previously that application of NMR to study the interactions between PEP-19 and apo CaM was severely limited since resonances for most backbone amides were broadened beyond detection in the apo CaM/PEP-19 complex (13). This was not due to the interaction of PEP-19 with the N-domain of CaM since amide chemical shifts in the N-domain are unaffected by PEP-19 binding (see Supplemental Figure 1). We felt that use of the isolated C-domain of CaM (C-CaM) may overcome this limitation due to different rotational correlation times (time)or other factors relative to intact CaM. This strategy was justified based on previous studies showing that the isolated C-domain of CaM (C-CaM) retains the biochemical properties of the intact protein (29–32). In addition, we showed that PEP-19 binds preferentially to the C-domain of CaM in the absence or presence of Ca^{2+}, and that PEP-19 has the same effects on the Ca^{2+} k_{off} rate of both C-CaM and intact CaM (13,14). Thus, the initial goal of the current study was to determine if amide resonances in apo C-CaM can be observed upon binding PEP-19. Indeed, addition of PEP-19 to apo C-CaM allowed observation of slow, two-state exchange for most amides. Backbone assignments for apo C-CaM bound to PEP-19 were obtained by HNCA, HN(CO)CA, HNCACB, CBCA(CO)NH, ^{15}N HSQC-TOCSY and ^{15}N-edited NOESY-HSQC experiments. All backbone amides were assigned except for Asp131 and Gly134, which are undetectable due to line broadening.

We next determined if C-CaM provided a good structural mimic of the C-domain from intact CaM in the absence of PEP-19. Supplemental Figure 2 compares the ^{1}H-^{15}N HSQC spectra of C-CaM versus intact CaM in the presence and absence of Ca^{2+}. The spectra of C-CaM are greatly simplified due to the absence of amide cross peaks from residues in the N-domain of CaM. As expected, amide chemical shifts for residues at the N-terminus of C-CaM, including the N-terminal portion of helix E, exhibit greater average amide chemical shift differences ($\Delta\delta_{avg}$) relative to CaM due to lack of influence from the tethered N-domain (see Supplemental Figure 3). However, average $\Delta\delta_{avg}$ for residues 88–148 of C-CaM and intact CaM are 0.014 and 0.012 in the absence and presence of Ca^{2+}, respectively, which are within the error of these measurements and calculations. In addition, the secondary structures of C-CaM and the C-domain of intact CaM are in excellent agreement in the presence and absence of Ca^{2+} as determined by $^{13}C_{\alpha}$ secondary chemical shifts, ^{1}H-^{15}N NOESY-HSQC, $^{3}J_{HAHA}$, and the Chemical Shift Index (see Supplemental Table 1).

We next compared ^{1}H-^{15}N HSQC spectra for Ca^{2+}-bound C-CaM versus intact CaM at increasing concentrations of PEP-19 at 298 K. Residues in the N-domain of CaM are not affected by PEP-19 binding and most resonances in Ca^{2+}-bound C-CaM exhibit characteristics of fast to intermediate exchange when titrated with PEP-19. This allowed assignments of backbone amides by following the movement of cross peaks. Assignments were then verified by ^{1}H, ^{15}N NOESY-HSQC. All residues were assigned except for Thr110, Asn111, Gly113, Glu114, and Lys115, due to severe resonance line broadening. Supplemental Figure 4 shows that all amide cross peaks for Ca^{2+}-C-CaM bound to PEP-19 superimpose on resonances associated with the C-domain of intact CaM bound to PEP-19 except residues 78 to 82 at the N-terminus of C-CaM. Thus, binding PEP-19 induces similar conformations in the Ca^{2+}-bound forms of both C-CaM and the C-domain of intact CaM. Together, supplemental Figures 1 to 4 demonstrate that C-CaM is a valid structural model for the study of interactions between CaM and PEP-19 in the presence or absence of Ca^{2+}.

Characteristics of slow and fast exchange on the NMR time scale for C-CaM amide resonances during titration with PEP-19 in the absence and presence of Ca^{2+}, respectively,

are consistent with the kinetics of binding PEP-19. Observed exchange characteristics are dependent on the relationship between chemical exchange (k_{ex}) and the difference in frequency for amide resonances between the bound and free states ($\Delta\omega$). Fast exchange is observed if $k_{ex} > \Delta\omega$, while slow exchange is seen if $k_{ex} < \Delta\omega$ Based on this, we can conclude that $k_{ex} > 150\ s^{-1}$ in the presence of Ca^{2+}, and $k_{ex} < 20\ s^{-1}$ in the absence of Ca^{2+}. The k_{ex} will be largely determined by k_{off} during titration of C-CaM with PEP-19 since $k_{ex} = [PEP\text{-}19]_{free}*k_{on} + k_{off}$, and $[PEP\text{-}19]_{free}$ will be very low until its total level exceeds that of C-CaM in the NMR sample. Thus, the above partial limits of k_{ex} based on $\Delta\omega$ are reasonable since we know that k_{off} values are $400\ s^{-1}$ and $5\ s^{-1}$ for binding PEP-19 to CaM in the presence and absence of Ca^{2+}, respectively (13,14).

PEP-19 has a greater effect on the structure of apo versus Ca^{2+}-bound C-CaM

Black bars in Figure 1A show that binding PEP-19 causes relatively small $\Delta\delta_{avg}$ in Ca^{2+}-C-CaM at 298 K (see Supplemental Figure 5A for complete spectra). The largest values of $\Delta\delta_{avg}$ are seen for residues Met144 to Lys148 at the C-terminus, while amide resonances for residues Thr110 to Lys115 in the linker between sites III and IV are broadened beyond detection upon binding PEP-19. Experiments performed previously at 320 K with intact Ca^{2+}-CaM (14) showed very similar patterns of $\Delta\delta_{avg}$ (see grey bars in Figure 1A), except that resonances for residues Thr110 to Lys115 were observed. This temperature dependence indicates that significant conformational exchange occurs on the μs-ms timescale for residues at the end of helix F and the linker between helices F and G of Ca^{2+}-CaM when bound to PEP-19.

Figure 1B shows that binding PEP-19 causes much greater $\Delta\delta_{avg}$ in apo C-CaM compared to Ca^{2+}-bound C-CaM. Similar to Ca^{2+}-C-CaM, residues with the largest $\Delta\delta_{avg}$ in apo C-CaM are localized to helix F and the linker between helices F and G, but changes are also seen for residues 101–103 at the transition between β-strand and helical structures in Ca^{2+} binding site III. Figure 1C and D illustrate the binding interface between C-CaM and PEP-19 in the absence and presence of Ca^{2+} based on residues with $\Delta\delta_{avg}$>0.2 ppm.

Experiments were performed to determine if apo and Ca^{2+}-bound C-CaM have different secondary structures when bound to PEP-19 that could account for different magnitudes and patterns of chemical shift changes in Figures 1A and 1B. Supplemental Figure 6 and Supplemental Table 1 show that secondary structures in the C-domain of CaM are essentially identical in the presence and absence of Ca^{2+} or PEP-19. Moreover, the antiparallel β-sheet between loops III and IV in apo and Ca^{2+}-bound C-CaM remain intact when bound to PEP-19 based on the presence of long-range NOEs (d_{NN}) between Ile100 and Val136 (data not shown). The largest difference in secondary structure is observed for helix F, which terminates at Val108 in apo C-CaM when bound to PEP-19, but extends to Asn111 under all other conditions. These data, together with Figure 1, suggest that Ca^{2+}-bound C-CaM remains predominantly in an “open-like” conformation in the presence of PEP-19, but that binding PEP-19 may alter interhelical angles in apo C-CaM.

Effect of PEP-19 on Ca^{2+} binding cooperativity of C-CaM

We showed previously that PEP-19 increased Ca^{2+} k_{off} and k_{on} rates, and decreased the cooperativity of Ca^{2+} binding to the C-domain of intact CaM with out greatly affecting the K_d (14). Specifically, the macroscopic Ca^{2+} dissociation constants for the C-domain of CaM are $K_{d1} = 17\ \mu M$ and $K_{d2} = 0.4\ \mu M$. This indicates positive cooperativity since $K_{d1} > 4K_{d2}$, with a change in free energy due to cooperativity ($\Delta\Delta G_c$) of −3.4 kcal/mole. In the presence of PEP-19, $K_{d1} = 4.7\ \mu M$ and $K_{d2} = 2.0\ \mu M$, respectively, which demonstrates a significant loss of cooperativity, with $\Delta\Delta G_c = -1.3$ kcal/mole. Despite these changes in macroscopic binding constants and cooperativity, the overall K_ds for binding Ca^{2+} to the C-domain are

very similar in the presence or absence of PEP-19. We also showed that PEP-19 increased, the Ca^{2+} k_{off} rate of isolated C-CaM (14). Figure 2 uses fluorescence from Tyr99 and Tyr138 to show that PEP-19 also decreases the cooperativity of Ca^{2+} binding to C-CaM as indicated by a decreased Hill coefficient in the presence of PEP-19, but does not greatly affect the K_d for Ca^{2+} binding. Thus, the effects of PEP-19 on the C-domain of intact CaM are also seen for C-CaM.

To identify potential structural manifestations of decreased cooperativity, amide chemical shifts were monitored by a series of ^{1}H-^{15}N HSQC spectra collected during titration of C-CaM with Ca^{2+} in the absence or presence of PEP-19 at 298 K. Figure 3 uses Thr117 to demonstrate slow two-state exchange observed for amides resonances in the absence of PEP-19. At intermediate levels of Ca^{2+} (Figure 3B and Figure 3C), resonances for both 0-Ca^{2+} and 2-Ca^{2+} forms are observed with relative intensities that are proportional to their populations. No evidence for the 1-Ca^{2+} form is observed at intermediate Ca^{2+} levels in the absence of PEP-19, indicating highly cooperative Ca^{2+} binding.

Figure 4 shows that fast to intermediate exchange on the NMR chemical timescale is observed upon titration of C-CaM with Ca^{2+} in the presence of PEP-19. Peaks corresponding to residues in Ca^{2+} binding sites III and IV, and helices E and F have large Ca^{2+}-dependent changes in amide chemical shifts that could not be detected at intermediate Ca^{2+} titration points due to line broadening. However, residues such as Thr117 that experience smaller overall Ca^{2+}-dependent amide chemical shift changes, could be observed at all Ca^{2+} levels. The NMR spectral characteristics for Thr117 in Figure 4A show resonance line broadening and splitting into multiple peaks at low Ca^{2+} levels, indicating rapid exchange between multiple conformations. Moreover, during titration with Ca^{2+}, Thr117 exhibits a biphasic change with an upfield shift in the ^{1}H dimension between Ca^{2+}/C-CaM ratios of 0 and 1.0, and then a downfield shift in the ^{15}N dimension at Ca^{2+}/C-CaM ratios between 1.0 and 2.0. These data are consistent with decreased cooperativity of Ca^{2+} binding in the presence of PEP-19 that results in significant populations of the 1-Ca^{2+} form of C-CaM at substoichiometric levels of Ca^{2+}.

Gly98 and Gly134 at the sixth position of loops III and IV, respectively, were selected to provide information on the sequential nature of Ca^{2+} binding to C-CaM in the presence of PEP-19. These glycines provide markers for Ca^{2+} binding since they facilitate the unusual main chain conformation that allows the Ca^{2+} ligands to take up coordinating positions (33). The large differences in amide chemical shifts of Gly98 and Gly134 between apo and Ca^{2+}-bound forms lead to severe resonance broadening at intermediate Ca^{2+} levels. However, Figure 4B shows that the change in chemical shift for Gly134 is maximal at a Ca^{2+}/C-CaM ratio of around 1.0, while the change in chemical shift for Gly98 is not maximal until a Ca^{2+}/C-CaM ratio of 2.0. These data indicate that PEP-19 promotes preferential binding of the first Ca^{2+} to site IV. However, Figure 4B shows that Gly98 in site III experiences minor conformational change upon binding the first Ca^{2+} to site IV, and binding the second Ca^{2+} to site III sharpens the line width of Gly134 in site IV. The simplest interpretation of these data is that PEP-19 decreases, but does not eliminate cooperativity between sites III and IV.

Effects of PEP-19 on the backbone dynamics of C-CaM

To better understand the effects of PEP-19 on backbone dynamics in C-CaM, ^{15}N relaxation experiments for apo and Ca^{2+}-bound C-CaM were collected in the absence or presence of PEP-19. The [^{1}H]-^{15}N NOE is typically most sensitive to motions on the ps –ns timescale, with values near 1.0 indicating a lack of such motions, and lower values indicating increasing local flexibility of the polypeptide. Similar to previous reports (15,17,34), Figure 5A and 5F show significant reductions in NOE values for residues at the N- and C- terminus of C-CaM in the presence or absence of Ca^{2+}. The two Ca^{2+} binding loops and the linker

between helix F and helix G also show lower NOE values. Binding PEP-19 had no significant effect on NOE values for apo- or Ca^{2+}-bound C-CaM (see Table 1). This confirms the results in Supplemental Table 1 showing that C-CaM/PEP-19 complexes have well-defined backbone structures.

Figure 5 and Table 1 show that binding PEP-19 to C-CaM causes an overall decrease in R_1, and an increase in R_2 in the presence or absence of Ca^{2+}. A molecular rotational correlation time (τ_m) of 4.8 ns is estimated from R_2/R_1 ratios for free apo and Ca^{2+}-bound C-CaM (see Table 1). This is consistent with the τ_m of 4.9 ns determined by Malmendal et al. (15) for apo C-CaM using the mean η_{xy}/η_z ratio and Model-Free analysis. The estimated τ_m for C-CaM is increased to 8.3 ns when bound to PEP-19 in the presence or absence of Ca^{2+}. The τ_m ratio of 1.73 for PEP-19/C-CaM versus free C-CaM is comparable their molecular weight ratio of 1.77, which suggests that the complexes are close to globular in shape. Residues with unusually high R_2/R_1 ratios relative to the average indicate regions that undergo conformational exchange processes on the μs-ms timescale (35). The R_1R_2 product is an effective discriminator of motional anisotropy and chemical/conformational exchange (36). Figure 5D and 5I show the R_2R_1 product, and Figures 5E and 5J show R_2/R_1 ratios for residues in apo and Ca^{2+}-bound C-CaM in the presence or absence of PEP-19. Table 2 lists residues with R_2/R_1 and R_1R_2 values that are both greater than 1SD relative to the average.

The Model-Free approach to predict residues with R_{ex} was not used since 3D structures of C-CaM/PEP-19 complexes are not available, and isotropic conditions cannot be assumed. Instead, the relaxation data were further analyzed using reduced spectral density mapping. The advantage of this approach lies in the absence of assumptions made *a priori* regarding internal motions and molecular tumbling (25,26). Reduced spectral density mapping assumes that the high- frequency spectral density terms are approximately equal in magnitude (i.e. $J(\omega_H \pm \omega_N) \approx J(\omega_H)$) and therefore may be replaced by a single value, $J(\omega_H)$. Reduced spectral density terms $J(\omega_H)$, $J(\omega_N)$ and $J(0)$ were calculated according to Eqs. (3)–(7) (see Materials and Methods) for apo and Ca^{2+}-bound C-CaM in the presence and absence of PEP-19, as summarized in Table 1 and Figure 6. $J(\omega_H)$ is correlated with fast internal motion of N-H bond vectors on the ps-ns timescale. Since the value of the area under $J(\omega)$ curve is constant, highly flexible segments of the backbone are characterized by high $J(\omega_H)$ values and low values of $J(0)$ and $J(\omega_N)$. This is observed for the N- and C-termini, and the linker between helices F and G of C-CaM. Figure 6A and D show that PEP-19 has relatively little effect on $J(\omega_H)$ for residues in C-CaM in the presence or absence of Ca^{2+}. This indicates little effect of PEP-19 on backbone dynamics of C-CaM on ps-ns timescale, and is consistent with a lack of effect of PEP-19 on heteronuclear NOEs.

An increase in molecular weight due to complex formation will globally increase $J(0)$, however, residues with unusually high $J(0)$ values relative to the average in a given protein or complex indicates significant chemical/conformational exchange on the μs- ms timescale due to contributions from R_{ex} on R_2 (25,26,37). Figure 7 shows residues in C-CaM with $J(0)$ values that are increased relative to the average $J(0)$ based on the expression $(J(0)–J(0)_{avg})/SD$. For example, Figure 7A shows that $J(0)$ values are increased by more than 1 SD relative to $J(0)_{avg}$ for Arg90, Phe92, Tyr99, Ile100, Thr110, Asp131, and Glu139. These same residues were shown by Malmendal et al. (15) to have the greatest R_{ex} based on Model-Free analysis. Interestingly, Figure 7 shows that binding PEP-19 causes large variations in $J(0)$ for residues in C-CaM in the presence or absence of Ca^{2+}. Residues in Table 2 that are highlighted in bold exhibit conformational exchange based on severe line width broadening., or $J(0)$, R_2/R_1, and R_1R_2 values that are all greater than one SD from the average.

DISCUSSION

Calmodulin is an essential and versatile Ca^{2+}-sensor capable of interacting with numerous target proteins, however, its intrinsic biochemical properties become limiting in cells that have very rapid Ca^{2+} oscillations, high total Ca^{2+} levels, numerous CaM binding proteins and limiting levels of CaM. This explains the need for proteins that can act as regulators of CaM signaling, or RCS proteins, to allow CaM to respond to diverse Ca^{2+} signals and achieve its wide array of known activities. We showed that the small neuronal IQ-motif proteins PEP-19 (62 a.a.) and RC3 (78 a.a.) modulate the Ca^{2+} binding properties of CaM (12,38). Another small neuronal protein called ARPP-21 (88 a.a.) was shown to inhibit CaM binding to target proteins (39). These activities could exert broad effects on cell activities. Indeed, ARPP-21 regulates Ca^{2+}-channel activity in mammalian brain, and RC3 plays a role in learning and memory (39–45). PEP-19 is thought to have cytoprotective activity based on its pattern of expression in cells that are affected by Alzheimer's (6) and Huntington's diseases (7), and expression of PEP-19 inhibits apoptosis and cell death due to Ca^{2+} overload (8,9). PEP-19 is of particular interest since it is expressed in non-neuronal tissues including endocrine, reproductive, and urinary organs that have highly active Ca^{2+} dynamics (46).

Diverse effects on essential cellular activities highlight the biological significance of PEP-19, ARPP-21 and RC3, and the need to understand their mechanisms of action. We showed previously that PEP-19 greatly increased the k_{on} and k_{off} rates for Ca^{2+} binding to the C-domain of CaM, with no change of apparent Ca^{2+} binding affinity (12), and that it decreased the cooperativity of Ca^{2+} binding (14). Changes in the cooperativity and kinetics of Ca^{2+} binding could result from static or dynamic properties of the CaM/PEP-19 complex. Dynamic properties are of particular interest since it is well-known that protein motions on the μs-ms timescale are often coupled with protein function (47–50), and the rate of Ca^{2+} exchange in the C-domain of CaM is correlated with rates of protein conformational exchange (15,18,51). The disordered nature of PEP-19 is significant since it could form so-called "Fuzzy" complexes (52), in which bound PEP-19 remains partially disordered to induce conformational exchange in CaM, and since disordered regions in proteins have been shown to enhance allosteric effects (53). These relationships led us to characterize the effect of PEP-19 on backbone dynamics of C-CaM, and to provide the experimental evidence for changes in cooperative Ca^{2+} binding at the atomic level.

It is well established that the C-domain of CaM binds 2 Ca^{2+} with a high degree of cooperativity (12,31,54–56). Figure 3 shows that this cooperativity results in apparent slow exchange of amide resonances during titration with Ca^{2+} such that cross peaks for only the 0-Ca^{2+} and 2-Ca^{2+} forms are observed at all Ca^{2+}/C-CaM ratios. In contrast, intermediate exchange is observed when C-CaM is titrated with Ca^{2+} in the presence of PEP-19, resulting in severe broadening of most amide cross peaks at intermediate Ca^{2+} levels. Amides for residues in the linker region between Ca^{2+} binding sites III and IV, and near the N- and C-termini are observed at lower contour levels at all Ca^{2+}/C-CaM ratios, and many of these residues, including Thr117 shown in Figure 4, exhibit a shift in the direction of the resonance migration at $[Ca^{2+}]/[\text{C-CaM}] > 1.0$. The simplest explanation for this is that PEP-19 decreases the cooperativity of Ca^{2+} binding to C-CaM, which allows a significant population of 1-Ca^{2+} form of PEP-19/C-CaM complex to accumulate at low Ca^{2+} levels. The effects of Ca^{2+} on amide cross peaks for Gly98 in Ca^{2+} binding site III and Gly134 in Ca^{2+} binding site IV indicate that Ca^{2+} binds preferentially to site IV in the presence of PEP-19. This Ca^{2+} binding preference is generally consistent with Malmendal et al. (15) who concluded that Ca^{2+} binds preferentially to site IV of unmodified free CaM at very low Ca^{2+} levels. Decreased cooperativity may be intrinsically linked to the effects of PEP-19 on Ca^{2+} k_{on} and k_{off} rates based on a mathematical model in which binding the first Ca^{2+} ion to

either site III or IV is characterized by fast rate constants, while binding the second Ca^{2+} occurs with much slower rates due to cooperative effects (14). This implies that attenuation of cooperativity by PEP-19 will increase Ca^{2+} binding rate constants by allowing greater expression of rapid rates associated with independent binding to site III or IV.

We used several criteria to identify residues in apo and Ca^{2+}-bound C-CaM that experience conformational/chemical exchange (R_{ex}) in the presence or absence of PEP-19. Residues indicated by bold lettering in Table 2 are those that experience severe exchange broadening, or that show significant conformational exchange based on high $J(0)$ values from reduced spectral density mapping, as well as high values for R_2/R_1 and R_1R_2. Figure 8A shows that residues with significant R_{ex} in apo C-CaM bound to PEP-19 are localized to Ca^{2+}-binding loop IV and the short β-strands between loops III and IV. In contrast, Figure 8B shows that residues 109 to 117 in helix F and the linker between helices F and G of Ca^{2+}-C-CaM show conformational exchange in the presence of PEP-19. This pattern of residues with R_{ex} differs from the effect of a peptide from transcription factor SEF2-1, which induces R_{ex} primarily in residues 142–147 at the C-terminus of Ca^{2+}-CaM (57). It also differs from the effect of binding a CaMKI peptide to Ca^{2+}-CaM, which causes relatively small R_{ex} in residues 102, 105–107 and 109 (58).

The pattern of residues with R_{ex}, and the k_{on} and k_{off} rates for binding PEP-19 to CaM, suggest that conformational exchange is derived from different mechanisms for apo and Ca^{2+}-bound C-CaM. Residues with R_{ex} in the apo C-CaM/PEP-19 complex are primarily localized to Ca^{2+} binding site IV, however, this does not correspond to the PEP-19 binding site, which is localized primarily to residues 108–117 based on amide chemical shift mapping shown in Figure 1. This suggests that R_{ex} is not due to intermolecular chemical exchange between apo C-CaM and PEP-19, but to intramolecular conformational exchange within the apo CaM/PEP-19 complex. This is consistent with k_{on} and k_{off} rates of 1 $\mu M^{-1}s^{-1}$ and 5.6 s^{-1}, respectively, for binding PEP-19 to apo CaM (13). Under conditions used for relaxation measurements, these rates give an estimated k_{ex} for intermolecular chemical exchange of about 200 s^{-1}, which is at the limit of the time frame that would give rise to R_{ex}. On the other hand, k_{on} and k_{off} rates for binding PEP-19 to Ca^{2+}-CaM are least 20 $\mu M^{-1}s^{-1}$ and 400 s^{-1}, respectively (13) These rates give a k_{ex} of least 4,500 s^{-1}, which is well within the range that would give rise to R_{ex}. In addition, residues with R_{ex} in the Ca^{2+}-C-CaM/PEP-19 complex are localized to the PEP-19 binding site. This suggests that conformational exchange induced by PEP-19 in Ca^{2+}-bound C-CaM is due to intermolecular chemical exchange.

The effects of PEP-19 on the cooperativity and k_{on} and k_{off} rates of Ca^{2+} binding to CaM may involve residues that experience conformational exchange on the slow timescale. The structural basis for cooperativity Ca2+ binding is primarily associated with two structural features of paired EF hands. The first is the antiparallel β-sheet formed between short β-strands in Ca^{2+} binding sites III and IV. This structure is also formed in other paired EF-hands, and was proposed as a conduit that transmits structural changes between Ca^{2+} binding sites in calbindin D_{9k} (59). Residues in the β-sheet region of apo C-CaM, but not Ca^{2+}-C-CaM, show increased R_{ex} when bound to PEP-19, including Ala102 in the strand/helix junction of Ca^{2+} binding loop III, and a cluster of residues across EF-hand IV. This supports a model in which PEP-19 increases the Ca^{2+} k_{on} rate by inducing conformational fluctuations in regions that lead to decreased Ca^{2+} binding cooperativity and preferential binding of Ca^{2+} to site IV. The second structural feature is the polypeptide linker between helix F of Ca^{2+}-binding site III and helix G in site IV of CaM. This strong covalent coupling would transmit conformational changes when the first Ca^{2+} binds to either site III or IV (60). PEP-19 induces R_{ex} for residues in this region of Ca^{2+}-bound, but not apo C-CaM, which may reflect coupling between protein dynamics and the Ca^{2+} k_{off} rate. Another

potential mechanism for increasing the Ca^{2+} k_{off} rate involves Asp93, which has increased R_{ex} in Ca^{2+}-bound C-CaM in the presence of PEP-19. The side chain carboxyl group of Asp93 contributes the *+X* ligand for coordination of Ca^{2+} at site III, and also forms a hydrogen bond with Phe89 ($Asp93H_N \rightarrow Phe89C'$) (61) that stabilizes the otherwise unfavorably close proximity of the negatively charged oxygen atoms in the co-ordination sphere of the bound Ca^{2+}. Conformational exchange at Asp93 in the presence of PEP-19 may increase the Ca^{2+} k_{off} rate.

In summary, the results presented here fill a gap in our understanding of how binding to proteins affects dynamic processes in CaM, by characterizing the effects of an intact, intrinsically disordered protein that binds with relatively low affinity but selectively to the C-domain of CaM in the presence or absence of Ca^{2+}. Binding PEP-19 has no effect on CaM backbone dynamics on the fast ns-ps timescale, but increases conformational exchange on the slow μs-ms timescale, and patterns of residues that exhibit conformational exchange differ significantly for apo versus Ca^{2+}-CaM. The data provide structural and dynamic evidence to support models in which PEP-19 decreases the degree of Ca^{2+} binding cooperativity in the C-domain of CaM and accelerates Ca^{2+} k_{on} and k_{off} rates with no change of apparent Ca^{2+} binding affinity.

Supplementary Material

Refer to Web version on PubMed Central for supplementary material.

Acknowledgments

This work was supported in part by training fellowships from the Keck Center Nanobiology Training Program of the Gulf Coast Consortia (NIH Grant No. R90 DK071504), and the American Heart Association, South Central Affiliate (10POST3110010), and by grants from the Welch Foundation (AU-1144), the NIH (R01 GM069611), and the American Heart Association, South Central Affiliate (GRNT2280427).

Abbreviations

CaM	calmodulin
C-CaM	isolated C-domain of CaM
EDTA	2,2′,2″,2‴-(ethane-1,2-diyldinitrilo)tetraacetic acid
EGTA	ethylene glycol-bis(2-aminoethylether)-*N*,*N*,*N*′,*N*′-tetraacetic acid
HEDTA	*N*′-(2-hydroxyethyl)ethylenediamine-*N*,*N*,*N*′-triacetic acid
NTA	nitrilotriacetic acid
DSS	2,2-dimethyl-2-silapentane-5-sulphonate
3D	three-dimensional
HSQC	heteronuclear single-quantum coherence spectroscopy
R_1	longitudinal relaxation rate constant
R_2	transverse relaxation rate constant
NOE	Nuclear Overhauser effect
SD	standard deviation
$\Delta\delta_{avg}$	average amide chemical shift change
τ_m	rotational correlation time

R_{ex}	chemical/conformational exchange

References

1. Rhoads A, Bahler M. Calmodulin signaling via the IQ motif. FEBS Lett. 2002; 513:107–113. [PubMed: 11911888]
2. Gerendasy DD. Homeostatic tuning of the Ca2+ signal transduction by members of the calpacitin protein family. J Neurosci Res. 1999; 58:107–119. [PubMed: 10491576]
3. Reck-Peterson SL, Provance WDJ, Mooseker MS, Mercer JA. Class V myosins. Biochim Biophys Acta. 2000; 1496:36–51. [PubMed: 10722875]
4. Jurado LA, Sethu P, Chockalingam PS, Jarrett HW. Apocalmodulin. Physiol Rev. 1999; 79:661–681. [PubMed: 10390515]
5. Hartmann J, Konnerth A. Determinants of postsynaptic Ca2+ signaling in Purkinje neurons. Cell Calcium. 2005; 37:459–466. [PubMed: 15820394]
6. Slemmon JR, Feng B, Erhardt JA. Small proteins that modulate calmodulin-dependent signal transduction: Effects of PEP-19, neuromodulin, and neurogranin on enzyme activation and cellular homeostasis. Molecular Neurobiology. 2000; 22:99–113. [PubMed: 11414283]
7. Utal AK, Stopka AL, Roy M, Coleman PD. PEP-19 immunohistochemistry defines the basal ganglia and associated structures in the adult human brain, and is dramatically reduced in Huntington's disease. Neuroscience. 1998; 86:1055–1063. [PubMed: 9697113]
8. Erhardt JA, Legos JJ, Johanson RA, Slemmon JR, Wang X. Expression of PEP-19 inhibits apoptosis in PC12 cells. Neuroreport. 2000; 11:3719–3323. [PubMed: 11117479]
9. Kanazawa Y, Makino M, Morishima Y, Yamada K, Nabeshima T, Shirakaki Y. Degradation of PEP-19 calmodulin-binding protein by calpain is implicated in neuronal cell death induced by intracellular Ca2+ overload. Neuroscience. 2008; 154:473–481. [PubMed: 18502590]
10. Kanamori T, Takakura K, Mandai M, Kariya M, Fukuhara K, Kusakari T, Momma C, Shime H, Yagi H, Konishi M, Suzuki A, Matsumura N, Nanbu K, Fujuita N, Fujii S. PEP-19 overexpression in human uterine leiomyoma. Mol Hum Repro. 2003; 9:709–717.
11. Ross, DTea. Systematic variation in gene expression in human cancer cell lines. Nat Genet. 2000; 24:208–209. [PubMed: 10700165]
12. Putkey JA, Kleerekoper Q, Gaertner TR, Waxham MN. A new role for IQ motif proteins in regulating calmodulin function. J Biol Chem. 2003; 278:49667–49670. [PubMed: 14551202]
13. Kleerekoper Q, Putkey JA. PEP-19: An instrinsically disordered regulator of CaM signaling. J Biol Chem. 2009; 284:7455–7464. [PubMed: 19106096]
14. Putkey JA, Waxham MN, Gaertner TA, Brewer KJ, Goldsmith M, Kubota Y, Kleerekoper QK. Acidic/IQ motif regulators of calmodulin. J Biol Chem. 2008; 283:1401–1410. [PubMed: 17991744]
15. Malmendal A, Evenas J, Forsen S, Akke M. Structural dynamics in the C-terminal domain of calmodulin at low calcium levels. J Mol Biol. 1999; 293:883–899. [PubMed: 10543974]
16. Zhang M, Tanaka T, Ikura M. Calcium-induced conformational transition revealed by the solution structure of apo-calmodulin. Nature Struct Biol. 1995; 2:758–767. [PubMed: 7552747]
17. Tjandra N, Kuboniwa H, Ren H, Bax A. Rotational dynamics of calcium-free calmodulin studieed by 15N-NMR relaxation measurements. Eur J Bioch. 1995; 230:1014–1024.
18. Evenas J, Malmendal A, Akke M. Dynamics of the transition between open and closed conformations in a calmodulin C-terminal domain mutant. Structure. 2001; 9:185–195. [PubMed: 11286885]
19. Peersen OB, Madsen TS, Falke JJ. Intermolecular tuning of calmodulin by target peptides and proteins: Differential effects on Ca2+ binding and implications for kinase activation. Protein Sci. 1997; 6:794–807. [PubMed: 9098889]
20. Putkey JA, Slaughter GR, Means AR. Bacterial expression and characterization of proteins derived from the chicken calmodulin cDNA and a calmodulin processed gene. J Biol Chem. 1985; 260:4704–4712. [PubMed: 2985564]

21. Putkey JA, Waxham MN. A peptide model for calmodlin trapping by calcium/calmodulin-dependent protein kinase II. J Biol Chem. 1996; 271:29619–29623. [PubMed: 8939892]
22. Xiong LW, Kleerekoper QK, Wang X, Putkey JA. Intra- and interdomain effects due to mutation of calcium-binding sites in calmodulin. J Biol Chem. 2010; 285:8094–8103. [PubMed: 20048169]
23. Farrow NAR, Muhandiram R, Singer AU, Pascal SM, Kay CM, Gish G, Shoelson SE, Pawson T, Forman-Kay JD, Kay LE. Backbone dynamics of a free and phosphopeptide-complexed Src homology 2 domain studied by 15N NMR relaxation. Biochemistry. 1994; 33:5984–6003. [PubMed: 7514039]
24. Wishart DS, Bigam CG, Yao J, Abildgaard F, Dyson HJ, Oldfield E, Markley JL, Sykes BD. H-1, C-13 and N-15 Chemical-Shift Referencing in Biomolecular Nmr. J Biomol Nmr. 1995; 6:135–140. [PubMed: 8589602]
25. Farrow NA, Zhang O, Szabo A, Torchia DA, Kay LE. Spectral density function mapping using 15N relaxation data exclusively. J Biomol NMR. 1995; 6:153–162. [PubMed: 8589604]
26. Sahu SC, Bhuyan AK, Majumdar A, Udgaonkar JB. Backbone dynamics of barstar: a (15)N NMR relaxation study. Proteins. 2000; 41:460–474. [PubMed: 11056034]
27. Kay LE, Torchia DA, Bax A. Backbone Dynamics of Proteins As Studied by 15N Inverse Detected Heteronuclear NMR Spectroscopy: Application to Staphylococcal Nuclease. Biochemistry. 1989; 28:8972–8979. [PubMed: 2690953]
28. Mercier P, Spyracopoulos L, Sykes BD. Structure, dynamics, and thermodynamics of the structural domain of troponin C in complex with the regulatory peptide 1–40 of troponin I. Biochemistry. 2001; 40:10063–10077. [PubMed: 11513585]
29. Evans TI, Shea MA. Energetics of calmodulin domain interactions with the calmodulin binding domain of CaMKII. Proteins. 2009; 76:47–61. [PubMed: 19089983]
30. VanScyoc WS, Sorensen BR, Rusinova E, Laws WR, Ross JB, Shea MA. Calcium binding to calmodulin mutants monitored by domain-specific intrinsic phenylalanine and tyrosine fluorescence. Biophys J. 2002; 83:2767–2780. [PubMed: 12414709]
31. Linse S, Helmersson A, Forsén S. Calcium binding to calmodulin and its globular domains. J Biol Chem. 1991; 266:8050–8054. [PubMed: 1902469]
32. Bayley PM, Findlay WA, Martin SR. Target recognition by calmodulin: Dissecting the kinetics and affinity of interaction using short peptide sequences. Protein Sci. 1996; 5:1215–1228. [PubMed: 8819155]
33. Strynadka NC, James MN. Crystal structures of the helix-loop-helix calcium-binding proteins. Annu Rev Biochem. 1989; 58:951–998. [PubMed: 2673026]
34. Barbato G, Ikura M, Kay LE, Pastor RW, Bax A. Backbone dynamics of calmodulin studied by 15N relaxation using inverse detected two-dimensional NMR spectroscopy: The central helix is flexible. Biochemistry. 1992; 31:5269–5278. [PubMed: 1606151]
35. Clore GM, Driscoll PC, Wingfield PT, Gronenborn AM. Analysis of the backbone dynamics of interleukin-1 beta using two-dimensional inverse detected heteronuclear 15N-1H NMR spectroscopy. Biochemistry. 1990; 29:7387–7401. [PubMed: 2223770]
36. Baudier J, Deloulme JC, Van Dorsselaer A, Black D, Matthes HW. Purification and characterization of a brain-specific protein kinase C substrate, neurogranin (p17). Identification of a consensus amino acid sequence between neurogranin and neuromodulin (GAP43) that corresponds to the protein kinase C phosphorylation site and the calmodulin-binding domain. J Biol Chem. 1991; 266:229–237. [PubMed: 1824695]
37. Peng JW, Wagner G. Frequency spectrum of NH bonds in eglin c from spectral density mapping at multiple fields. Biochemistry. 1995; 34:16733–16752. [PubMed: 8527448]
38. Gaertner TR, Putkey J, Waxham MN. Kinetics of calmodulin binding to RC3/neurogranin. Soc Neurosci Abst. 2002:30.
39. Rakhilin SV, Olson PA, Nishi A, Starkove NN, Fienberg AA, Nairn AC, Surmeier DJ, Greengard P. A network of control mediated by regulator of calcium/calmodulin-dependent signaling. Science. 2004; 306:698–701. [PubMed: 15499021]
40. Miyakawa T, Yared E, Pak JH, Huang FL, Huang KP, Crawley JN. Neurogranin null mutant mice display performance deficits on spatial learning tasks with anxiety related components. Hippocampus. 2001; 11:763–775. [PubMed: 11811671]

41. Wu J, Li L, Huang K-P, Huang FL. Attenuation of protein kinase C and cAMP-dependent protein kinase signal transduction in the neurogranin knockout mouse. J Biol Chem. 2002; 277:19498–19505. [PubMed: 11912190]

42. Krucker T, Siggins GR, McNamara RK, Lindsley KA, Dao A, Allison DW, De Lecea L, Lovenberg TW, Sutcliffe JG, Gerendasy DD. Targeted disruption of RC3 reveals a calmodulin-based mechanism for regulating metaplasticity in the hippocampus. Journal of Neuroscience. 2002; 22:5525–5535. [PubMed: 12097504]

43. Englander WS. Protein folding intermediates and pathways studied by hydrogen exchange. Annu Rev Biomol Struct. 2000; 29:213–238.

44. Pak JH, Huang FL, Li J, Balschun D, Reymann KG, Chiang C, Westphal H, Huang K-P. Involvement of neurogranin in the modulation of calcium/calmodulin-dependent protein kinase II, synaptic plasticity, and spatial learning: A study with knockout mice. Proc Natl Acad Sci U S A. 2000; 97:11232–11237. [PubMed: 11016969]

45. Huang FL, Huang KP, Wu J, Boucheron C. Environmental enrichment enhances neurogranin expression and hippocampal learning and memory but fails to rescue the impairments of neurogranin null mutant mice. J Neurosci. 2006; 26:6230–6237. [PubMed: 16763030]

46. Ge X, Yamamoto S, Tsutsumi S, Midorikawa Y, Ihara S, Wang SM, Aburatani H. Interpreting expression profiles of cancers by genome-wide survey of breadth of expression in normal tissues. Genomics. 2005; 86:127–141. [PubMed: 15950434]

47. Palmer AG, CDK, Loria JP. Nuclear magnetic resonance methods for quantifying microsecond-to-millisecond motions in biological macromolecules. Meth Enz. 2001:339.

48. Mittermaier A, Kay LE. New tools provide new insights in NMR studies of protein dynamics. Science. 2006; 312:224–228. [PubMed: 16614210]

49. Boehr DD, Dyson HJ, Wright PE. An NMR perspective on enzyme dynamics. Chem Rev. 2006; 106:3055–3079. [PubMed: 16895318]

50. Kern D, Eisenmesser EZ, Wolf-Watz M. Enzyme dynamics during catalysis measured by NMR spectroscopy. Methods Enzymol. 2005; 394:507–524. [PubMed: 15808235]

51. Evenas J, Forsen S, Malmendal A, Akke M. Backbone dynamics and energetics of a calmodulin domain mutant exchanging between closed and open conformations. J Mol Biol. 1999; 289:603–617. [PubMed: 10356332]

52. Tompa P, Fuxreiter M. Fuzzy complexes: polymorphism and structural disorder in protein-protein interactions. Trends Biochem Sci. 2008; 33:2–8. [PubMed: 18054235]

53. Hilser VJ, Thompson EB. Intrinsic disorder as a mechanism to optimize allosteric coupling in proteins. Proc Natl Acad Sci U S A. 2007; 104:8311–8315. [PubMed: 17494761]

54. Biekofsky RR, Martin SR, Browne JP, Bayley PM, Feeney J. Ca2+ coodination to backbone carbonyl oxygen atoms in calmodulin and other EF-hand proteins: 15N chemical shifts as probes for monitoring individual-site Ca2+ coordination. Biochemistry. 1998; 37:7617–7629. [PubMed: 9585577]

55. Pedigo S, Shea MA. Discontinuous equilibrium titrations of cooperative calcium binding to calmodulin monitored by 1-D 1H-nuclear magnetic resonance spectroscopy. Biochemistry. 1995; 34:10676–10689. [PubMed: 7654722]

56. Crouch TH, Klee CB. Positive cooperative binding of calcium to bovine brain calmodulin. Biochemistry. 1980; 19:3692–3698. [PubMed: 7407067]

57. Larsson G, Schleucher J, Onions J, Hermann S, Grundstrom T, Wijmenga SS. Backbone dynamics of a symmetric calmodulin dimer in complex with the calmodulin-binding domain of the basic-helix-loop-helix transcription factor SEF2-1/E2-2: a highly dynamic complex. Biophys J. 2005; 89:1214–1226. [PubMed: 15894636]

58. Frederick KK, Kranz JK, Wand AJ. Characterization of the backbone and side chain dynamics of the CaM-CaMKIp complex reveals microscopic contributions to protein conformational entropy. Biochemistry. 2006; 45:9841–9848. [PubMed: 16893184]

59. Nelson MR, Thulin E, Fagan PA, Forsen S, Chazin WJ. The EF-hand domain: a globally cooperative structural unit. Protein Sci. 2002; 11:198–205. [PubMed: 11790829]

60. Gifford JL, Walsh MP, Vogel HJ. Structures and metal-ion-binding properties of the Ca2+-binding helix-loop-helix EF-hand motifs. Biochem J. 2007; 405:199–221. [PubMed: 17590154]

61. Juranic N, Atanasova E, Streiff JH, Macura S, Prendergast FG. Solvent-induced differentiation of protein backbone hydrogen bonds in calmodulin. Protein Sci. 2007; 16:1329–1337. [PubMed: 17567747]

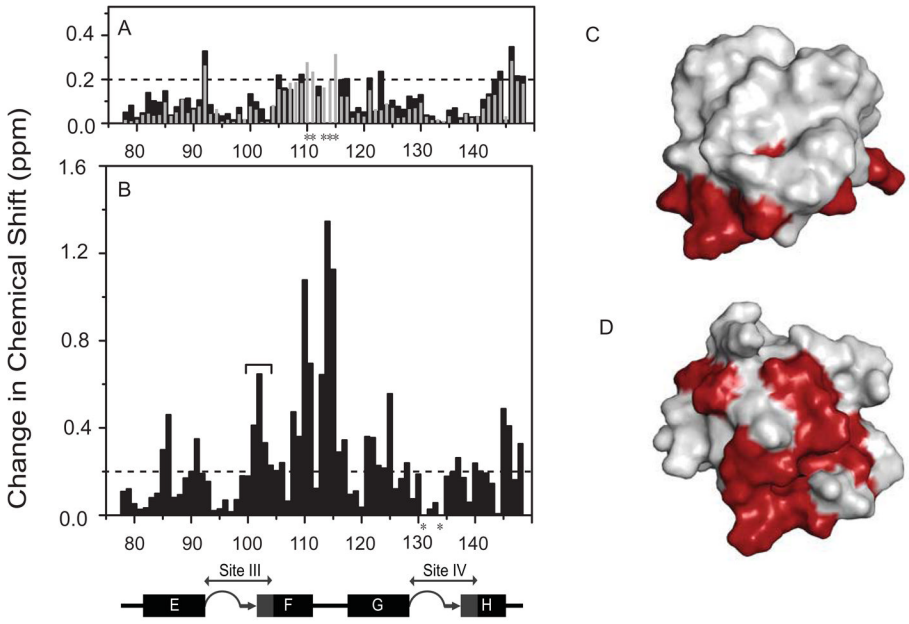

Figure 1. Effect of PEP-19 on C-CaM amides in the absence and presence of Ca^{2+}

(A) Amide chemical shift perturbations ($\Delta\delta_{avg}$) for Ca^{2+}-bound C-CaM at 298 K are shown by black bars. Grey bars show $\Delta\delta_{avg}$ that result from binding PEP-19 to the C-domain of intact Ca^{2+}-CaM at 320 K (14). Asterisks denote resonances with significant line-broadening in the presence of PEP-19. ***(B)*** $\Delta\delta_{avg}$ for apo C-CaM at 298 K. Panels ***(C)*** and ***(D)*** map residues with $\Delta\delta_{avg}$ >0.2 ppm on the solvent accessible surfaces of Ca^{2+}-CaM (pdb:1J7P) and apo-C-CaM (pdb:1F71), respectively. The structures are presented in the same relative orientation. The diagram below panel B shows the relative positions of the helices E to H in the primary sequence of CaM. The 12 amino acids Ca^{2+} binding sites III and IV are also shown in grey. Coil, β-strand and α-helical portions of these structures are indicated by loops, arrows, and boxes, respectively.

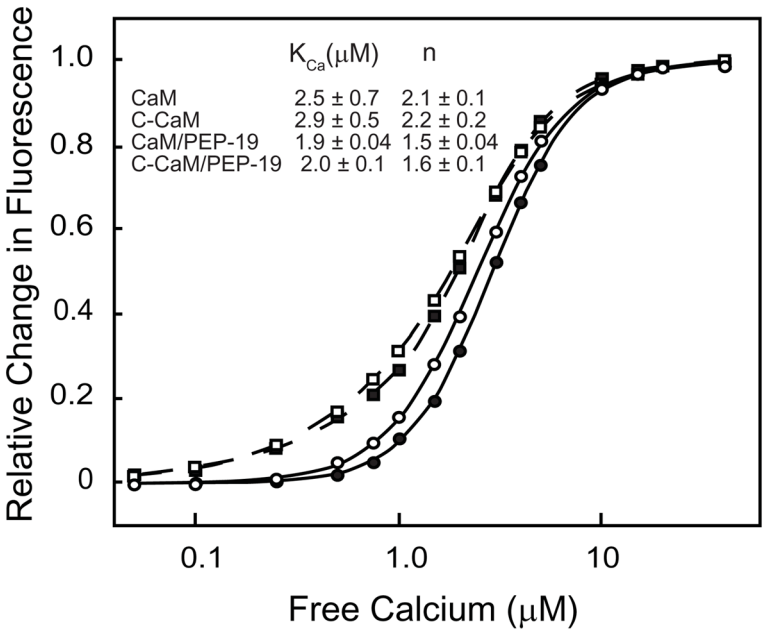

Figure 2. Effect of PEP-19 on the Ca^{2+} binding constant (K_{ca}) and Hill coefficient (n)

Intrinsic tyrosine fluorescence was monitored during titration of CaM (○), CaM+PEP-19 (□), C-CaM (●), and C-CaM/PEP-19 (■) with Ca^{2+}. The lines show fits of the data to the Hill equation (Eq.1).

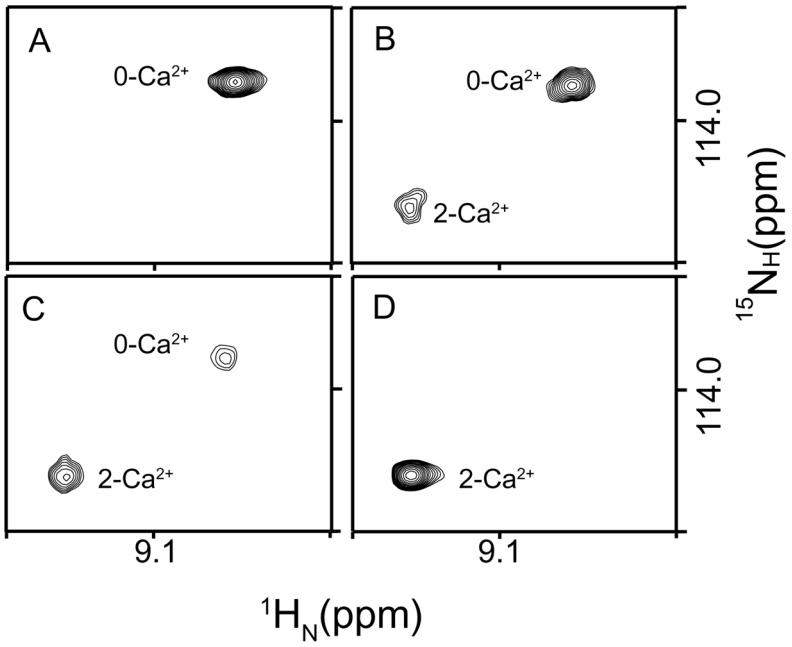

Figure 3. Ca^{2+} -dependent changes in amide chemical shifts of C-CaM show strong cooperativity
Resonance of Thr117 in the linker region of C-CaM exhibited two-state slow exchange at various molar ratio of Ca^{2+} added into C-CaM, indicating highly cooperative Ca^{2+} binding to sites III and IV. ***(A)*** [Ca^{2+}]/[C-CaM]=0; ***(B)*** [Ca^{2+}]/[C-CaM]=0.3; ***(C)*** [Ca^{2+}]/[C-CaM]=0.6; ***(D)*** [Ca^{2+}]/[C-CaM]=2.0.

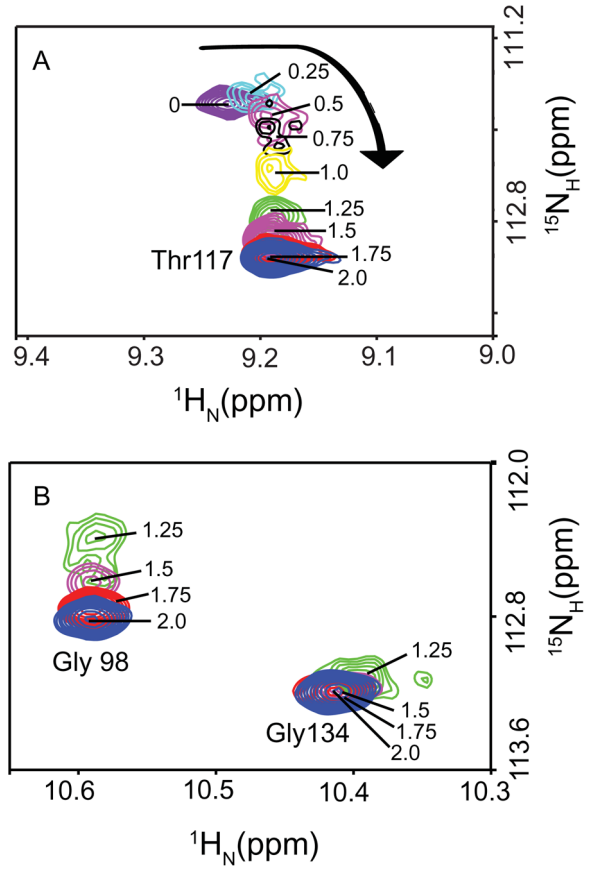

Figure 4. Ca^{2+} -dependent changes in amide chemical shifts of C-CaM in the presence of PEP-19 show decreased cooperativity

Various ratios of [Ca^{2+}]/[C-CaM] between 0 and 2.0 are indicated. Exchange characteristics for Thr117 shown in ***Panel (A)*** indicate lower degree of cooperativity of Ca^{2+} binding in the presence of PEP-19. Exchange characteristics for Gly98 in Ca^{2+} binding site III and Gly134 in the Ca^{2+} binding site IV shown in ***Panel (B)*** indicates preferential binding of the 1st Ca^{2+} to site IV.

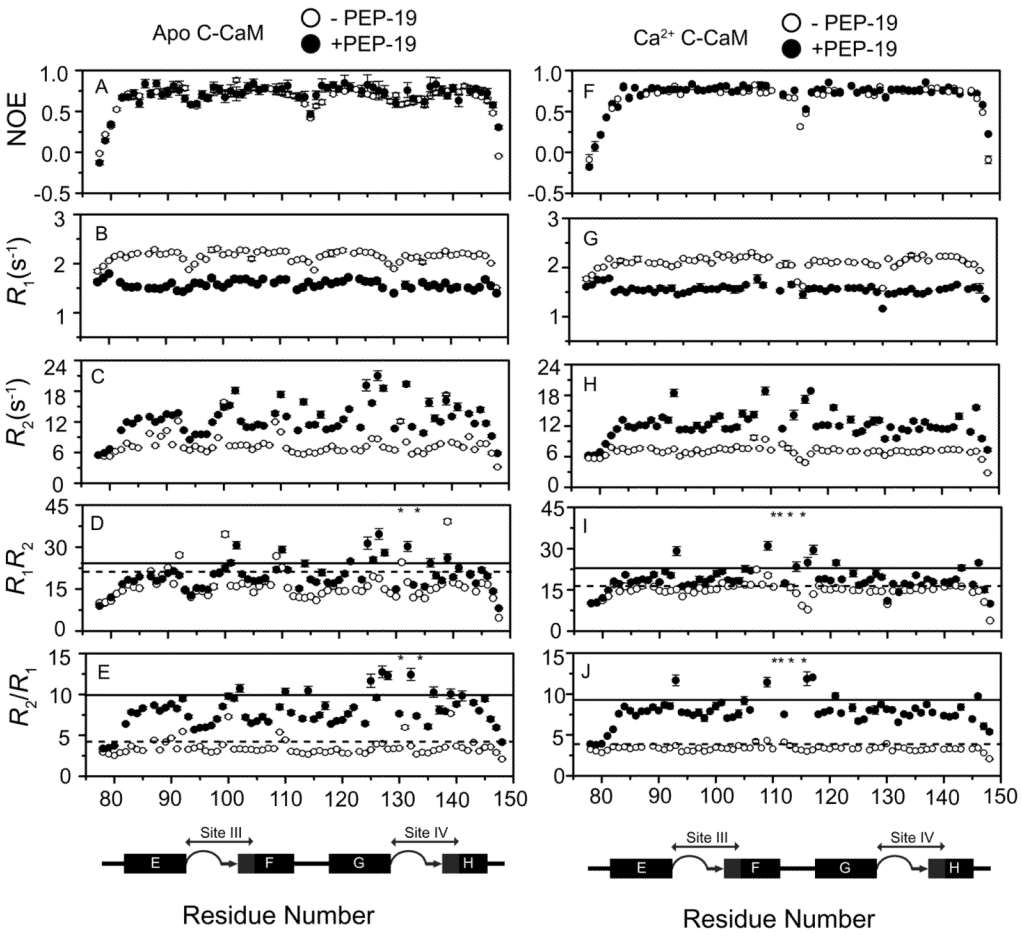

Figure 5. Backbone ^{15}N relaxation parameters for apo C-CaM, apo C-CaM/PEP-19, Ca^{2+}-bound C-CaM and Ca^{2+}-bound C-CaM/PEP-19

R_1, R_2, [^{1}H]-^{15}N NOE, R_2R_1 products and R_2/R_1 ratios are shown for apo- and Ca^{2+}-C-CaM in the absence (open circles) and presence (closed circles) of PEP-19. The dashed (with out PEP-19) and solid lines (with PEP-19) in Panels C, D, G and H indicate the mean +1.0 SD. Asterisks denote resonances with significant line-broadening in the presence of PEP-19.

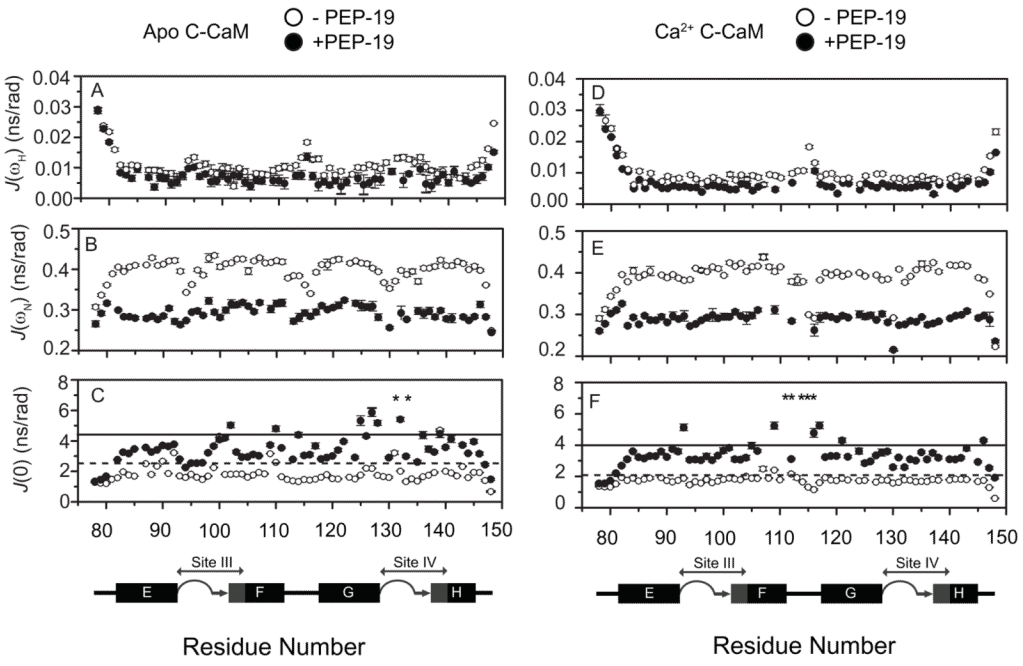

Figure 6. Reduced spectral density mapping for apo C-CaM, apo C-CaM/PEP-19, Ca^{2+}-bound C-CaM and Ca^{2+}-bound C-CaM/PEP-19

Reduced spectral density parameters were calculated using Eq. (3) to Eq. (7). $J(\omega_H)$, $J(\omega_N)$, and $J(0)$ are shown for apo- and Ca^{2+}-C-CaM in the absence (open circles) and presence (closed circles) of PEP-19. The mean +1.0 SD of $J(0)$ for apo and Ca^{2+}-bound C-CaM in the absence and presence of PEP-19 is indicated by dash and solid line, respectively. Asterisks denote resonances with significant line-broadening in the presence of PEP-19.

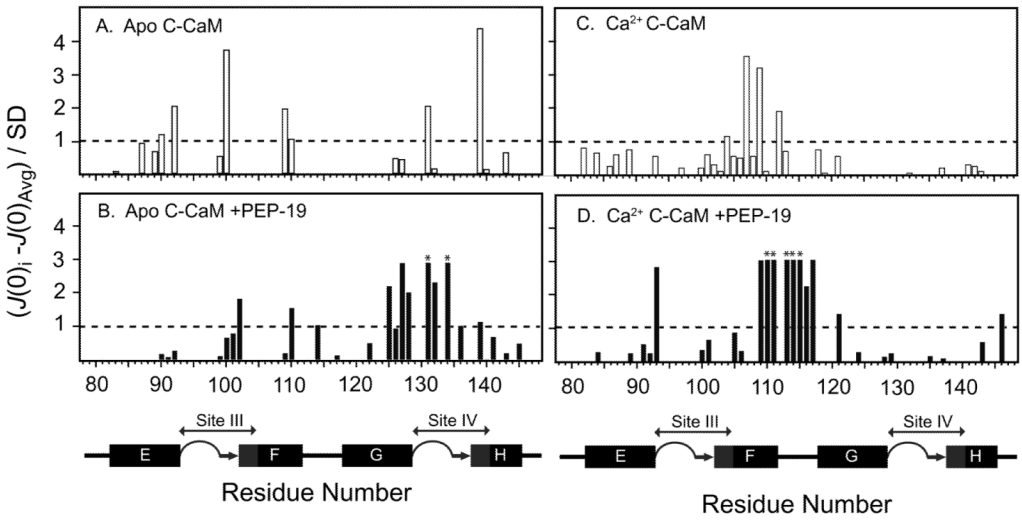

Figure 7. Identification of residues exhibiting conformational exchange on the μs –ms timescale in PEP-19-bound apo C-CaM and Ca^{2+}-C-CaM based on reduced spectral density mapping

Values on the Y-axis are calculated by $(J(0)_i - J(0)_{avg})/SD$. Residues with $(J(0)_i - J(0)_{avg})/SD$ >1.0 are considered to undergo significant chemical/conformational exchange. Asterisks indicate residues with extreme line broadening.

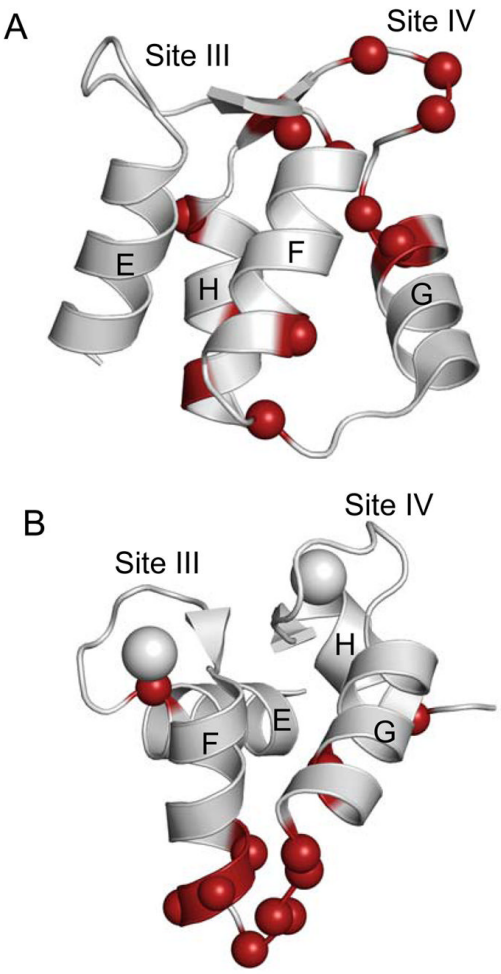

Figure 8. Summary of residues that exhibit significant conformational exchange for apo and Ca^{2+}-bound C-CaM in the presence of PEP-19

Panels (A) and ***(B)*** show the NMR solution structures for apo (pdb: 1F71) and Ca^{2+}-bound C-domain of CaM (pdb: 1J7P), respectively. Colored balls indicate residues that exhibit significant conformational exchange, and are shown by bold lettering in Table 2.

Table 1

Summary of R_1, R_2, NOE, R_1R_2, R_2/R_1, τ_m, $J(0)$, $J(\omega_N)$, and $J(\omega_H)$

Protein	^{15}N relaxation parameters			R_1R_2	R_2/R_1	τ_m	reduced spectral density mapping		
	R_1	R_2	NOE				$J(0)$	$J(\omega_N)$	$J(\omega_H)$
	s^{-1}	s^{-1}				ns	ns/rad	ns/rad	ns/rad
Apo C-CaM	2.14±0.13	7.6±2.2	0.67±0.16	16.3±5.2	3.51±0.96	4.83±0.46	1.88±0.64	0.40±0.03	0.011±0.004
Apo C-CaM +PEP-19	1.58±0.085	12.5±3.2	0.70±0.17	19.7±5.2	7.93±2.00	8.33±0.66	3.40±0.92	0.29±0.017	0.008±0.004
Ca^{2+} C-CaM	2.09±0.17	7.1±1.0	0.68±0.19	14.8±2.7	3.36±0.33	4.81±0.19	1.74±0.26	0.39±0.04	0.010±0.005
Ca^{2+} C-CaM +PEP-19	1.56±0.091	12.2±2.5	0.70±0.18	18.9±4.1	7.82±1.60	8.38±0.37	3.08±0.79	0.29±0.014	0.009±0.007

Table 2

Summary of Residues that Undergo Conformational Exchange on the μs-ms Timescale

Protein	R_2/R_1		R_2R_1		Reduced Spectral Density Mapping		Exchange Broadening	
Apo C-CaM	**Glu87 Arg90 Phe92 Ile100**	**Met109 Thr110 Asp131 Glu139**	**Glu87 Arg90 Phe92 Ile100**	**Met109 Thr110 Asp131 Glu139**	**Glu87 Arg90 Phe92 Ile100**	**Met109 Thr110 Asp131 Glu139**		
Apo C-CaM +PEP-19	**Ala102 Thr110 Glu114 Ile125 Glu127**	**Ala128 Gly132 Val136 Glu139**	**Ala102 Thr110 Glu114 Asp122 Ile125** Arg126	**Glu127 Ala128 Gly132 Val136 Glu139**	**Ala102 Thr110 Glu114 Ile125 Glu127**	**Ala128 Gly132 Val136 Glu139**	**Asp131 Gly134**	
Ca^{2+}-C-CaM	Asp93 **Glu104 His107 Met109**	**Leu112** Gly113 Ile130	Ser101 **Glu104 His107**	**Met109 Leu112**	**Glu104 His107**	**Leu112 Met 109**		
Ca^{2+}-C-CaM +PEP-19	**Asp93 Met109 Leu116**	**Thr117 Val121 Thr146**	**Asp93 Met109 Leu116 Thr117**	**Val121** Gln143 **Thr146**	**Asp93 Met109 Leu116**	**Thr117 Val121 Thr146**	**Thr 110 Asn111 Gly 113**	**Glu114 Lys115**

Residues exhibiting conformational exchange on the μs-ms timescale by all criteria are shown in bold.